


# Approaching the Thouless energy and Griffiths regime in random spin systems by singular value decomposition

Wen-Jia Rao <sup>\*</sup>*School of Science, Hangzhou Dianzi University, Hangzhou 310027, China*

(Received 11 October 2021; revised 7 December 2021; accepted 11 February 2022; published 22 February 2022)

We employ singular value decomposition (SVD) to study the eigenvalue spectra of random spin systems. By SVD, eigenvalue spectrum is decomposed into orthonormal modes  $W_k$  with weight  $\lambda_k$ . We show that the scree plot ( $\lambda_k$  with respect to  $k$ ) in the ergodic phase contains two branches that both follow power law  $\lambda_k \sim k^{-\alpha}$  but with different exponents  $\alpha$ . By evaluating  $W_k$ , we verified the part of  $\lambda_k$  with  $k > k_{\text{Th}}$  is universal that follows random matrix theory, where  $k_{\text{Th}}$  is related to the Thouless energy. We further demonstrate that  $\alpha$  corresponds only to the exponential part of the level spacing distribution while being insensitive to the level repulsion, or equivalently the system's symmetry. Consequently,  $\alpha$  gives an underestimation for the many-body localization transition point, which suggests a nonergodic behavior that may be attributed to the Griffiths regime.

DOI: [10.1103/PhysRevB.105.054207](https://doi.org/10.1103/PhysRevB.105.054207)

## I. INTRODUCTION

The quantum phases of matter in isolated systems is a focus of modern condensed matter physics where the existence of two generic phases has been well established: an ergodic phase and a many-body localized (MBL) phase [1,2]. In an ergodic phase, the system acts as the heat bath for its subsystem, which results in extensive quantum entanglement that follows volume law. In contrast, a MBL phase is where localization persists in the presence of weak interactions, which leads to area-law entanglement. The different scaling behaviors of quantum entanglement provide the modern understanding about these two phases [3–11].

On the other hand, the ergodic and MBL phases are traditionally distinguished by their eigenvalue statistics [12–20] whose foundation is laid by the random matrix theory (RMT) [21,22]. RMT is a powerful mathematical tool that describes the universal properties of the eigenvalues in the ergodic phase which depend only on the system's symmetry while independent of microscopic details. Specifically, the Gaussian orthogonal/unitary ensemble (GOE/GUE) describes systems with/without time reversal symmetry, and Gaussian symplectic ensemble (GSE) stands for time-reversal invariant systems with broken spin rotational invariance. On the contrary, the eigenvalues in MBL phase are independent of each other and belong to the Poisson ensemble.

Compared to the properties of each phase, the evolution between them is much less understood, especially on the ergodic side. There are two issues of particular interest. The first one concerns the energy scale called Thouless energy  $E_{\text{Th}}$ , defined through the Thouless time  $t_{\text{Th}} = \hbar/E_{\text{Th}}$ , which measures the average time a particle takes to diffuse over the system. Therefore, eigenvalue fluctuations below  $E_{\text{Th}}$  are well characterized by RMT and hence universal, while those above  $E_{\text{Th}}$  are model dependent. This energy scale  $E_{\text{Th}}$  is difficult to

observe with local spectral statistics such as level spacing or spacing ratio distributions, but can be probed by long-range spectral measures such as the number variance [23–25] or spectral form factor [26–29]. The second issue regards the Griffiths regime near the transition region [30–34], where an inhomogeneous mixture of locally thermal and localized regions coexist and result in anomalously slow dynamics and multifractality of eigenstates. Unlike the Thouless energy, the study of the Griffiths effect is normally based on eigenfunctions.

In this work, we employ the singular-value decomposition (SVD) to study the eigenvalue spectra of random spin systems with MBL transition and show that both the Thouless energy and Griffiths regime can be revealed through the scaling of singular values. The advantages of this method are two-fold. For the Thouless energy, SVD requires no unfolding procedure, which is necessary for studying number variance and the spectral form factor, and therefore avoids the potential ambiguity raised by the concrete unfolding strategy [35]. Very recently, Berkovits employed SVD to the study of Thouless energy in the Anderson model [24] and the identification of a nonergodic extended phase in the Rosenzweig-Porter model [25,36]. We now bring it to the many-body regime. For the Griffiths effect, the inputs of SVD are the eigenvalue spectra, which are numerically much easier to obtain than the eigenfunctions.

The underlying mechanism behind SVD is to view the eigenvalue spectrum of a complex quantum system as a time series [37–43] and by performing SVD to the “sample matrix” [see Eq. (2) in Sec. II] we are able to distinguish the trend and fluctuation modes therein. This technique is, in essence, identical to the unsupervised machine learning algorithm called principal component analysis (PCA), which has also found various applications in condensed matter physics [44–47]. However, while PCA deals with several components with the largest weights, we shall see the universal information of the MBL system is encoded in the intermediate components with lower weights.

<sup>\*</sup>wjr@hdu.edu.cn

This paper is organized as follows. In Sec. II we introduce the SVD method, and show the scree plot (singular values as a function of the level index) for the MBL phase reflects a clear integrable behavior, while that for the ergodic phase breaks into two branches—a universal high-order part that belongs to RMT and a nonuniversal part, with the starting point of the former identifying the Thouless energy  $E_{\text{Th}}$ . In Sec. III we dig into the structures of the principal components, show the higher-order ones are close to the Fourier modes of the eigenvalue spectrum, and explain why the higher-order part of the scree plot is universal. In Sec. IV we demonstrate that the scree plot only reflects the exponential part of the level spacing distribution while being insensitive to the level repulsion, or equivalently the system's symmetry. Consequently, as detailed in Sec. V, it gives an underestimation on the ergodic-MBL transition point, which suggests a nonergodic behavior that may be attributed to the Griffiths regime. A discussion and conclusion are presented in Sec. VI.

## II. SVD ON EIGENVALUE SPECTRA

In this work we consider the paradigmatic spin model with ergodic-MBL transition, that is, the antiferromagnetic Heisenberg model with random external fields [48], the Hamiltonian reads

$$H = \sum_{i=1}^L \mathbf{S}_i \cdot \mathbf{S}_{i+1} + \sum_{i=1}^L \sum_{\tau=x,y,z} h_{\tau} \varepsilon_i^{\tau} S_i^{\tau}, \quad (1)$$

where the coupling strength is set to be 1, and  $\varepsilon_i^{\tau}$  s are random variables within range  $[-1, 1]$ . We first consider the orthogonal case with time-reversal symmetry, that is,  $h_x = h_z = h \neq 0$  and  $h_y = 0$ , where an ergodic-MBL transition happens at  $h_c \simeq 3$  [14,15]. Using exact diagonalization, we generate  $N = 1000$  samples of eigenvalue spectra at various randomness  $h$  in an  $L = 13$  system, with the Hilbert space dimension being  $2^{13} = 8192$ . For each spectrum, we take out the middle  $P = 1000$  eigenvalues and arrange them into an  $N \times P$  matrix  $X$ ,

$$X = \begin{pmatrix} E_1^{(1)} & E_2^{(1)} & \dots & \dots & E_P^{(1)} \\ E_1^{(2)} & E_2^{(2)} & \dots & \dots & E_P^{(2)} \\ \vdots & \vdots & \ddots & \ddots & \vdots \\ \vdots & \vdots & \ddots & \ddots & \vdots \\ E_1^{(N)} & E_2^{(N)} & \dots & \dots & E_P^{(N)} \end{pmatrix}, \quad (2)$$

where  $E_i^{(j)}$  stands for the  $i$ th eigenvalue in the  $j$ th sample. For clarity, we shall call  $X$  the ‘‘sample matrix.’’ We then perform SVD on  $X$ , which equals reexpressing  $X$  as

$$X = U \Lambda W \equiv \sum_k \sigma_k X^{(k)}, \quad X_{ij}^{(k)} = U_{ik} W_{kj}, \quad (3)$$

where  $\Lambda$  is an  $N \times P$  matrix whose nonzero elements  $\Lambda_{i,i} \equiv \sigma_i$  are the ordered singular values  $\sigma_1 \geq \sigma_2 \geq \dots \geq \sigma_r$  with  $r \leq \min[N, P] = \text{Rank}[X]$ . This technique is equivalent to the machine learning algorithm called principal component analysis (PCA), the spirit of which is to view the eigenvalue spectrum as multi-dimensional data, and by SVD we decompose it into orthonormal modes  $W_k$ —the  $k$ th row of the  $P \times P$  matrix  $W$ —with weight  $\sigma_k$ . The  $W_k$  is called the principal

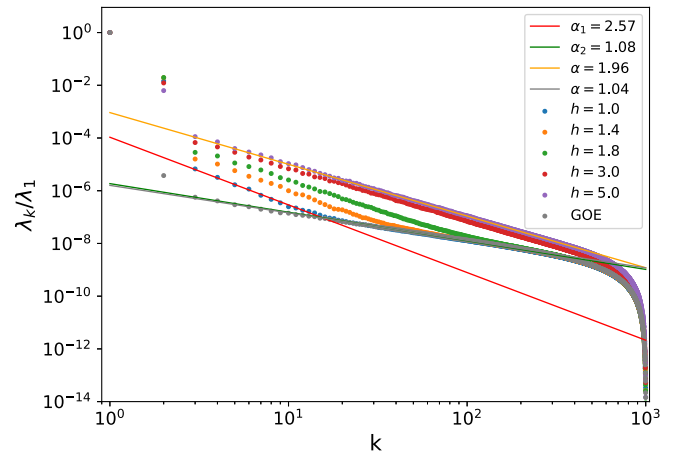


FIG. 1. Scree plots of  $\{\lambda_k/\lambda_1\}$  at various randomness strengths. Despite the two dominant modes,  $\lambda_k$  in the MBL phase ( $h = 5$ ) follows a power law  $k^{-\alpha}$  with  $\alpha \simeq 2$  reflecting the integrable behavior. Two-branch structures appear for  $\lambda_k$  in the ergodic phase ( $h < 3$ ), separating the model-dependent lower part and the universal higher part that belongs to RMT, the starting point of the higher part provides an estimation of the Thouless energy.

component in the terminology of PCA, and encodes one feature (character) of the eigenvalue spectrum whose physical meaning is read by evaluating its behavior  $W_k[i]$ , where  $i$  denotes the energy level index. Given the decreasing tendency of  $\sigma_k$ , we can approximate the original sample matrix  $X$  by  $\tilde{X} = \sum_{k=1}^m \sigma_k X^{(k)}$  with some value  $m$ , hence achieving the purpose of dimension reduction. In most applications of PCA, we only keep several dominant components with the largest weights. However, as we shall see, the universal information of the random spin system is encoded in the intermediate components with lower weights.

Another interpretation of SVD is to treat  $X$  as a multivariate time series, with  $\lambda_k \equiv \sigma_k^2$  being the eigenvalue of the covariance matrix  $X^T X$ . It was demonstrated [24,25,37] that  $\lambda_k$  with large  $k$  follows the power-law behavior

$$\lambda_k \sim \frac{1}{k^\alpha}, \quad (4)$$

with  $\alpha = 1(2)$  in the chaotic (integrable) system, corresponding to the ergodic (MBL) phase, respectively.

As a demonstration, we generate the sample matrix  $X$  for Eq. (1) with  $L = 13$  at various randomness strengths and plot the resulting  $\lambda_k$  after SVD with respect to index  $k$  (the so-called scree plot) in a log-log scale in Fig. 1. Without loss of generality, we divide each  $\lambda_k$  by the largest value  $\lambda_1$ . For comparison, we also generate eigenvalue spectra from modeling GOE matrices [orthogonal matrices with random elements drawn from standard Gaussian distribution  $N(0, 1)$ ] of the same size, the resulting  $\lambda_k/\lambda_1$  appear as the grey dots therein. Clearly, in all cases, the first two modes are orders of magnitudes larger than the rest, which indicates the existence of two overwhelming features in the eigenvalue spectrum. For reasons detailed in the next section, we identify them to be the mean energy  $\langle E \rangle$  and mean level spacing  $\langle s \rangle$ . While for large modes with  $k > 300$ , the weights drops very rapidly, indicating they contribute little to the properties of the eigenvalue

spectrum. The universal information is thus expected to be encoded in the intermediate modes with  $2 < k < 300$ .

More specifically, for the case in the MBL phase ( $h = 5$ ), the scree plots with  $3 \leq k \leq 200$  fits well into the power-law behavior Eq. (4) with  $\alpha = 1.962$ , very close to the value of 2 for the integrable system, as expected. While for data in the ergodic phase ( $h = 1$ ),  $\lambda_k$  divides into two parts: the higher-part  $30 \leq k \leq 200$  with power-law exponent  $\alpha_2 \simeq 1.085$  almost coincides with that of modeling GOE, reflecting a clear chaotic behavior, and this part is identified to be universal below Thouless energy and related to RMT; while the lower-part  $3 \leq k \leq 15$  follows a super-Poissonian power-law behavior with  $\alpha_1 \simeq 2.567$ , and is therefore identified to be the model-dependent part beyond Thouless energy. A more detailed analysis will be provided in Sec. III. Interestingly, this value of  $\alpha_1$  happens to be close to the one in the metallic phase of a three-dimensional (3D) Anderson model [24], which may suggest a subtle correspondence between these two models.

From Fig. 1 we can see such a two-branch scree plot is general for data in the ergodic phase, and quantitatively we identify the Thouless energy  $E_{\text{Th}}$  through the starting point of the chaotic behavior  $\lambda_k \sim k^{-1}$ , which is  $k_{\text{Th}} \sim 30$  for the case  $h = 1$ . As the randomness grows, the  $k_{\text{Th}}$  increases—which indicates  $E_{\text{Th}}$  decreases—and the two branches gradually get mixed. At the transition point  $h \simeq 3$ , the scree plot becomes almost identical to that of the MBL phase, suggesting the saturation of  $\alpha_2$  may be an indicator for the MBL transition. However, as discussed in detail in Sec. V, this may not provide an accurate estimation.

Up to now, we have shown the scree plots provides a transparent way to reveal the Thouless energy  $E_{\text{Th}}$ . However, since there is an artifact in determining where the chaotic behavior  $\lambda_k \sim k^{-1}$  begins to hold, this method is less accurate in quantitatively determining  $E_{\text{Th}}$  than more standard probes like the spectral form factor. Meanwhile, the numerics clearly indicate that  $E_{\text{Th}}$  decreases with randomness strength, which is qualitatively consistent with the results in Ref. [29]. Moreover, as stated in Sec. I, the central advantage of SVD is that it requires no unfolding procedure. To further pursue the physics behind the scree plot, we now turn to the analysis of the principal components  $W_k$ .

### III. PRINCIPAL COMPONENT ANALYSIS

The  $k$ th principal component of the eigenvalue spectrum is represented by the  $k$ th row of the matrix  $W$ , we therefore evaluate the behavior of  $W_k$  with respect to the energy level index  $i$  to read out the physics. The results in this section are based on the data from  $h = 1$ , and we checked they hold in other cases as well.

We saw in Fig. 1 that the scree plot is dominated by two largest weights  $\lambda_1$  and  $\lambda_2$ , which means the eigenvalue spectrum contains two dominant features that are overwhelming over other features. We therefore draw the behaviors of two dominant modes  $W_1$  and  $W_2$  in Fig. 2(a), it is clear that both of them are linearly dependent with level index  $i$ , suggesting they correspond to two nonfluctuating features of the eigenvalue spectrum. We postulate these two dominant features to be the mean energy  $\langle E \rangle$  and the mean level spacing  $\langle s \rangle$ , both of which are nonuniversal. To support this conjecture, we first

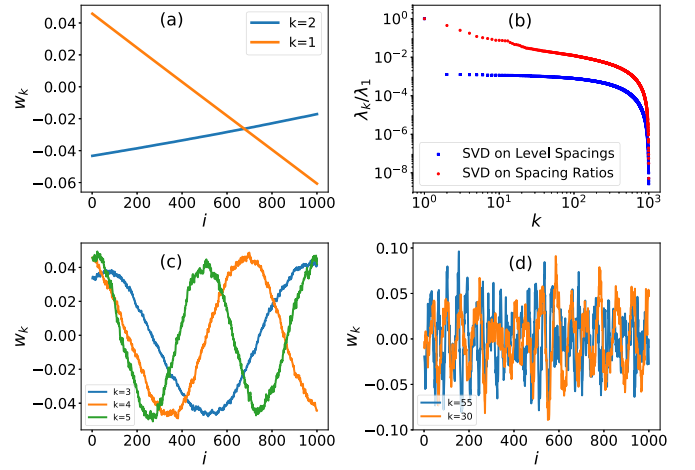


FIG. 2. (a) Behaviors of the two dominant components  $W_{1/2}$ —the linear behaviors indicate they correspond to two nonfluctuating features of the eigenvalue spectrum, which are suspected to be the mean energy  $\langle E \rangle$  and level spacing  $\langle s \rangle$ . (b) Scree plots of  $\lambda_k$  after performing SVD on the sample matrix comprised of level spacings and spacing ratios, where the ratio of first two weights  $\lambda_1/\lambda_2 = 789.14(2.25)$  in the respective cases. (c,d) Behaviors of typical higher components  $W_k$ . The quasiperiodic behaviors indicate they are close to the  $k$ th Fourier mode of the eigenvalues and the frequency increases with  $k$ .

change the input data from the eigenvalues  $\{E_i\}$  to the level spacings  $\{s_i = E_{i+1} - E_i\}$ . With this input, the information of the mean energy  $\langle E \rangle$  is lost, leaving  $\langle s \rangle$  as the only dominant feature. Therefore, when applying SVD to this new sample matrix  $X'$ , we should observe only one dominant weight  $\lambda_1$ . This is verified in Fig. 2(b), where  $\lambda_1/\lambda_2 = 789.14$  is observed. We can further change the input to be the spacing ratios  $\{s_{i+1}/s_i\}$ , where the information about  $\langle E \rangle$  and  $\langle s \rangle$  are both lost, and the resulting scree plot is expected to contain no dominant weights. This is also verified in Fig. 2(b), where we see  $\lambda_1$  is the same order with  $\lambda_2$  (the precise value is  $\lambda_1/\lambda_2 = 2.25$ ), which confirms our conjecture.

Strictly speaking, the mean energy  $\langle E \rangle$  and level spacing  $\langle s \rangle$  are nonuniversal for different reasons. The  $\langle E \rangle$  stands for the global energy scale of the system and therefore depends on the model's details. While  $\langle s \rangle$  is the value that can be artificially assigned when counting level statistics, which stems from the mathematical degree of freedom in the joint probability distribution function of the eigenvalues. To be specific, recall the eigenvalue distribution function in the standard WD class is [21,22]

$$P(\{E_i\}) = A_1 \prod_{i < j} |E_i - E_j|^\beta e^{-A_2 \sum_i E_i^2}; \quad \beta = 1, 2, 4, \quad (5)$$

where  $A_1$  and  $A_2$  are two parameters constrained by the single normalization condition  $\int P(\{E_i\}) \prod_i dE_i = 1$ . From  $P(\{E_i\})$  we can derive the celebrated WD distribution  $P(s) = A_1 s^\beta e^{-A_2 s^2/2}$  using the Wigner surmise [21,22]. The single normalization condition  $\int P(s) ds = 1$  is not sufficient to determine two parameters  $A_1, A_2$ , which gives us the freedom to choose  $\langle s \rangle$ . In most practical studies, we take  $\langle s \rangle$  to be 1.

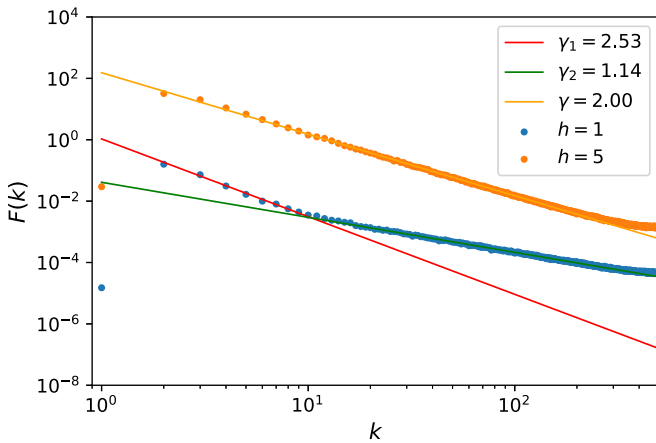


FIG. 3. Power spectrum function  $F(k)$  for ergodic ( $h = 1$ ) and MBL ( $h = 5$ ) phases. In the first a clear two-branch structure appears just like in the scree plot of  $\lambda_k$ . The power-law exponents  $\gamma \simeq \alpha$  are observed in all cases.

Having understood the physics of the two dominant components, we now return to analysis of the components  $W_k$  ( $k \geq 3$ ) of the original sample matrix  $X$ , several of which are plotted in Figs. 2(c) and 2(d). We observe clear sinusoidal behaviors of  $W_k$  with respect to level index  $i$ , with the frequency increasing with  $k$ . Specifically, we have  $W_k[i] \sim \cos(\frac{(k-1)\pi}{N}i + \varphi_k)$  with  $N = 1000$  being the number of eigenvalues, which indicates the component  $W_k$  is close to the  $k$ th Fourier mode of the eigenvalue spectrum. Therefore, for smaller  $k$ ,  $W_k$  reflects the level fluctuations on larger energy scale. When  $k$  is not so large, this energy scale goes beyond Thouless energy, so its behavior is nonuniversal; while when  $k$  exceeds certain threshold  $k_{\text{Th}}$ , this energy scale falls within the Thouless energy. This threshold  $k_{\text{Th}}$  divides the  $\lambda_k$  into two parts: the nonuniversal part with  $k < k_{\text{Th}}$  and universal part with  $k > k_{\text{Th}}$ . This is the origin of the two-branch structure of the scree plot in the ergodic phase.

The local fluctuations of the eigenvalue spectra can be further revealed by considering the power spectrum function whose definition is

$$F_m(k) = \left| \frac{1}{r} \sum_{n=1}^r \left[ \left( \sum_{p=3}^r \sigma_p X_{mn}^{(p)} \right) \exp\left(-\frac{2\pi ink}{r}\right) \right] \right|^2, \quad (6)$$

where  $\sum_{p=3}^r \sigma_p X_{mn}^{(p)}$  are the eigenvalue spectra after “global unfolding” [37–39]. By averaging over the ensemble we get the power spectrum function  $F(k) = \frac{1}{N} \sum_{m=1}^N F_m(k)$ , which was shown to behave differently in integrable and chaotic systems [24,37,40,49,50]. To this end, we calculate  $F(k)$  in the  $h = 1(5)$  case standing for the ergodic (MBL) phase. The results are shown in Fig. 3. As we can see  $F(k)$  behaves totally similar to  $\lambda_k$ : in the ergodic phase  $F(k)$  divides into two branches that both follow  $1/k^\gamma$ , specifically, the lower modes satisfy  $\gamma_1 \simeq 2.5 \simeq \alpha_1$  and higher modes satisfy  $\gamma_2 \simeq 1 \simeq \alpha_2$ ; while for the MBL case, a single curve with  $\gamma \simeq 2 \simeq \alpha$  appears. This coincidence has also appeared in the noninteracting Anderson model [24], which indicates that  $F(k)$  and  $\lambda_k$  essentially contain identical physical information.

Based on the PCA results above, we can provide a qualitative explanation as follows.

We verified that  $W_k$  is close to the Fourier modes of eigenvalue spectrum for  $k \geq 3$ , hence the power-law behavior  $\lambda_k \sim k^{-\alpha}$  essentially indicates a decreasing trend of the eigenvalues’ Fourier weights. On the other hand, the definition of  $F(k)$  in Eq. (6) drops the first two dominant terms  $X^{(1/2)}$ , which stand for the mean energy  $\langle E \rangle$  and level spacing  $\langle s \rangle$  that are both nonfluctuating. Therefore, the fluctuating behaviors of the original eigenvalue spectra and the one after “global unfolding” (that is,  $\sum_{p=3}^r \sigma_p X_{mn}^{(p)}$ ) should be the same. Consequently, the scaling behaviors of  $\lambda_k$  and  $F(k)$  are expected to be identical.

A technical issue worth mentioning is that the choice of power spectrum in Eq. (6) is not unique. Another routine is to construct the following time series [40–43]:

$$\delta_n = \sum_{i=1}^n (s_i - \langle s \rangle) = s_n - n\langle s \rangle, \quad (7)$$

where  $s_n$  is the  $n$ th-order level spacing. It is clear that  $\langle \delta_n \rangle$  gets rid of the nonuniversal information about  $\langle E \rangle$  and  $\langle s \rangle$ , in a similar way to  $\sum_{k=3}^r \sigma_k X_{ij}^{(k)}$  in Eq. (6), hence its Fourier weight  $S(k)$  shows totally similar behaviors to  $F(k)$  in Fig. 3. Despite these qualitative estimations, we also note the analytical derivation for  $S(k)$  was recently given in Refs. [51–53].

#### IV. RELATING $\alpha$ TO LEVEL SPACING DISTRIBUTION

Up to now, we demonstrated that the power-law exponent  $\alpha$  (which is  $\alpha_2$  in the ergodic phase) for  $\lambda_k$  with large  $k$  is universal that related to RMT. However, the power-law exponent  $\alpha$  is only a single number. It is still questionable whether it can distinguish different random matrix ensembles which may contain multiple parameters. For example, the general form of the level spacing distribution  $P(s)$  contains two parts: the polynomial part that reflects the level repulsion and an exponential part that reflects large  $s$  decaying. As for the random spin system, a widely used two-parameter spacing distribution for the ergodic-MBL transition was proposed by Serbyn and Moore [20], i.e.,

$$P(\beta_1, \beta_2, s) = C_1 s^{\beta_1} \exp(-C_2 s^{2-\beta_2}). \quad (8)$$

For the case deep in the ergodic phase, we have  $\beta_1 = 1, \beta_2 = 0$  standing for the GOE distribution; while for the case deep in the MBL phase,  $\beta_1 = 0, \beta_2 = 1$  for the Poisson ensemble. We conjecture that the power exponent  $\alpha$  of  $\lambda_k$  corresponds *only* to the parameter  $\beta_2$  in the exponential part, while being insensitive to the level repulsion  $\beta_1$ . If this conjecture is correct, two deductions are immediate: (i) the scree plot with  $\alpha = 2$  does not necessarily correspond to the Poisson ensemble, but also to a number of intermediate ensembles whose spacing distribution decays as  $e^{-Cs}$ ; (ii) the scree plot with  $\alpha = 1$  in ergodic phase is insensitive to the level repulsion, or equivalently, the symmetry of the system.

To verify (i), we consider the random matrix model called the short-range plasma model (SRPM) [54], which describes the eigenvalues as an ensemble of one-dimensional particles with only nearest-neighboring logarithmic interactions. SRPM holds the semi-Poisson distribution which is widely

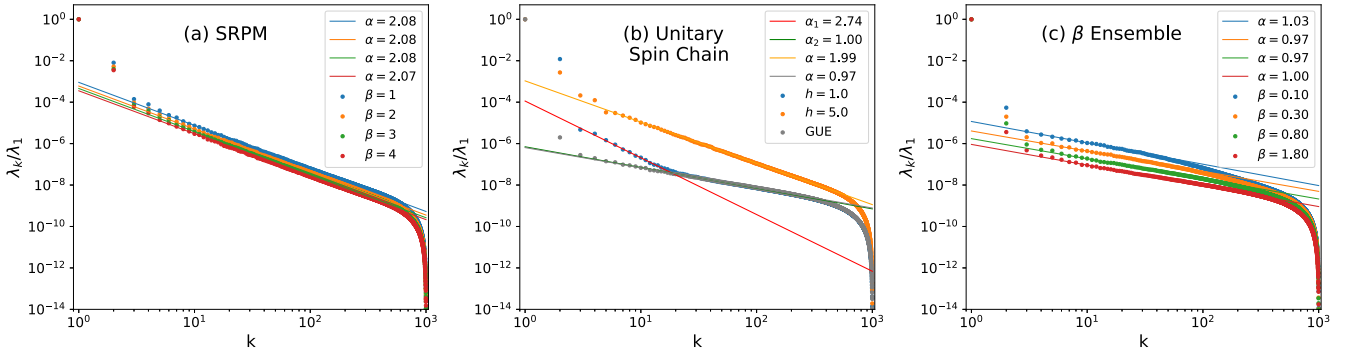


FIG. 4. (a)  $\{\lambda_k/\lambda_1\}$  of SRPM with different level repulsion  $\beta$ . The integrable behavior  $\lambda_k \sim k^{-2}$  appears in all cases. (b)  $\{\lambda_k/\lambda_1\}$  for the unitary spin system, the behaviors of both the ergodic ( $h = 1$ ) and MBL ( $h = 5$ ) phases are totally similar to those in the orthogonal system in Fig. 1, indicating the scree plot is insensitive to the system's symmetry. (c)  $\{\lambda_k/\lambda_1\}$  for the Gaussian  $\beta$  ensemble with several nonstandard values of  $\beta$ . Chaotic behavior  $\lambda_k \sim k^{-1}$  appears in all cases.

accepted as the critical distribution at the MBL transition point. It was shown [54] that the large  $s$  behavior of SRPM decays as  $s^\beta e^{-(\beta+1)s}$  with  $\beta$  being the Dyson index controlling the strength of level repulsion. Thus, if the deduction (i) holds, we should observe identical power-law exponents  $\alpha$  for cases with different  $\beta$ . To effectively obtain the eigenvalue spectrum of the SRPM, we make use of an elegant correspondence between SRPM and the Poisson ensemble, that is, the spectrum comprised of every  $(\beta + 1)$ th eigenvalue from the Poisson ensemble is identical to the eigenvalue spectrum of SRPM with index  $\beta$  [55]. Therefore, we can easily obtain the sample matrix of SRPM to perform SVD, and the resulting scree plots for  $\beta = \{1, 2, 3, 4\}$  are displayed in Fig. 4(a). As expected, the scree plots are totally similar, and the power-law exponent  $\alpha \simeq 2$  appears in all cases, which verifies (i).

For deduction (ii), we first consider a unitary spin system that breaks time-reversal symmetry, i.e., the case with  $h_x = h_y = h_z = h \neq 0$  in Eq. (1). This model undergoes an ergodic-MBL transition at around  $h_c \simeq 2.5$  [14,15], with the level spacing distribution evolving from GUE to Poisson. We likewise take  $h = 1$  and  $h = 5$  to represent the ergodic and MBL phases, respectively. With the same size of samples, we obtain the resulting scree plots shown in Fig. 4(b), where we also draw  $\{\lambda_k/\lambda_1\}$  from a modeling GUE for comparison. As can be seen,  $\lambda_k \sim 1/k$  appears in both the higher part of the ergodic phase and modeling GUE, which are totally similar to the cases in Fig. 1 and  $\lambda_k \sim 1/k^2$  appears for the data in the MBL phase, as expected. We further consider the Gaussian  $\beta$  ensemble which holds the same form of eigenvalue distribution as WD classes [Eq. (5)], but with  $\beta$  different from  $\{1, 2, 4\}$ . The eigenvalue spectra of the general Gaussian  $\beta$  ensemble can be efficiently generated by diagonalizing the following tridiagonal matrix [56]:

$$M_\beta = \frac{1}{\sqrt{2}} \begin{pmatrix} x_1 & y_1 & & & & & \\ y_1 & x_2 & & & & & \\ & & \ddots & & & & \\ & & & \ddots & & & \\ & & & & y_{N-2} & x_{N-1} & y_{N-1} \\ & & & & y_{N-1} & x_N & \end{pmatrix}, \quad (9)$$

where the diagonals  $x_i$  ( $i = 1, 2, \dots, N$ ) follow the normal distribution  $N(0, 2)$  and  $y_k$  ( $k = 1, 2, \dots, N - 1$ ) follows the  $\chi$  distribution with parameter  $(N - k)\beta$ . Without loss of generality, we select several nonstandard values of  $\beta$  and generate 1000 samples of eigenvalue spectrums with the matrix dimension  $N = 4000$  to construct the sample matrix  $X$ . The resulting scree plots are displayed in Fig. 4(c). We see the chaotic behavior  $\lambda_k \sim k^{-1}$  appears in all cases, as expected. Thus, combining Figs. 4(b) and 4(c) we confirm deduction (ii).

## V. EVOLUTION OF $\alpha_2$ DURING ERGODIC-MBL TRANSITION

Given the universal information of the system is encoded in the power exponent  $\alpha_2$  of the higher part of the scree plot, it is a natural idea to employ it to detect the ergodic-MBL transition, without referring to the study of eigenfunctions. We expect the exponent  $\alpha_2$  to evolve from 1 in the ergodic phase to 2 in the MBL phase. Specifically, we consider the orthogonal spin model Eq. (1) with length  $L = 13$  in the randomness range  $h \in [1, 5]$  with interval  $\delta h = 0.2$ . We generate 1000 samples of the eigenvalue spectra at each  $h$ , and select 1000 eigenvalues in the middle to construct the sample matrix  $X$  and hence obtain  $\lambda_k$ . The exponent  $\alpha_2$  is determined by fitting  $\lambda_k \sim k^{-\alpha_2}$  for  $50 < k < 250$  in all cases.

For comparison, we employ another eigenvalue-based quantity to detect the MBL transition, that is, the intersample randomness, whose definition goes as follows. First, we adopt a variant definition of spacing ratio, which is [12]

$$t_i = \frac{\min\{s_{i+1}, s_i\}}{\max\{s_{i+1}, s_i\}}, \quad (10)$$

where  $s_i = E_{i+1} - E_i$  is the  $i$ th level spacing. The mean value  $\bar{t}$  in different ensembles was calculated to be [57]  $\bar{t}_{\text{GOE}} = 0.536$  and  $\bar{t}_{\text{Poisson}} = 0.386$ . The calculation of  $\bar{t}$  contains two steps: first we calculate the mean spacing ratio  $t_S = \langle t_i \rangle_{\text{samp}}$  in one sample, then we average  $t_S$  over an ensemble of samples to get  $\bar{t} = \langle t_S \rangle_{\text{en}}$ . The two steps generate two types of variance. The first one is  $V_S = \langle t_S^2 \rangle_{\text{en}} - \bar{t}^2$ , i.e., the variance of a sample-averaged spacing ratio over the ensemble, which measures the intersample randomness. The second one is  $V_I = \langle v_I \rangle_{\text{en}}$  where  $v_I = \langle t_i^2 \rangle_{\text{samp}} - t_S^2$ , measuring the intrinsic intrasample

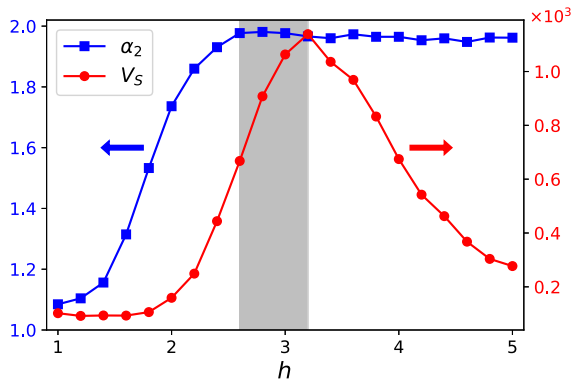


FIG. 5. Evolutions of  $V_S$  and the power-law exponent  $\alpha_2$  with respect to the randomness strength  $h$ . The grey shaded area represents a nonergodic region that may be attributed to the Griffiths regime.

randomness. In an MBL system driven by random disorder, such as Eq. (1), the distribution of  $t_S$  near the transition region will deviate from a Gaussian function—a manifestation of the Griffiths regime—which results in a peak of  $V_S$  at the transition point [58–60]. Therefore, we can compute the evolution of  $V_S$  to locate the transition.

The evolutions of  $V_S$  and  $\alpha_2$  are drawn collectively in Fig. 5. The peak of  $V_S$  identifies the transition point to be  $h_c \simeq 3.2$ , which is very close to the widely accepted value  $h_c \simeq 3$  [14,15], while  $\alpha_2$  saturates to 2 at roughly  $h = 2.6$ , smaller than the transition value. This clearly indicates a nonergodic region in the ergodic phase.

One explanation for this result is the existence of Griffiths regime close to the transition point that contains locally localized small regions. To be specific, the evolution of the spacing distribution in Eq. (8) during the ergodic-MBL transition was discussed by Serbyn and Moore [20], where they showed that the Griffiths effects affect the large  $s$  decaying of  $P(s)$  more than the small  $s$  behavior. Consequently, the parameter  $\beta_2$  becomes  $\beta_2 \sim 1$  even when the system is globally in the metallic phase. As demonstrated in the previous section,  $\alpha_2$  detects only the power exponent in the exponential part of  $P(s)$  (that is,  $\beta_2$ ), it is not surprising that  $\alpha_2$  saturates earlier than the transition happens. However, we cannot rule out other possibilities such as the existence of a nonergodic extended phase [61–65] without studying the distribution of eigenvectors. A possible way to gain further evidence would be to study the MBL system with the quasiperiodic potential that is

free of the Griffiths regime. It is intriguing to see whether  $\alpha_2$  will underestimate the transition point in such systems. This, however, goes beyond the scope of the current work.

## VI. CONCLUSION AND DISCUSSION

We employed the singular value decomposition (SVD) to study the eigenvalue spectra of the random spin systems. By treating the eigenvalue spectrum as a time series, we show the eigenvalue spectra are dominated by two nonuniversal features—the mean energy  $\langle E \rangle$  and level spacing  $\langle s \rangle$ , while the higher component  $W_k (k \geq 3)$  is close to the spectrum's  $k$ th Fourier mode. Consequently, the scree plot of the singular values  $\lambda_k$  in the ergodic phase exhibits a two-branch structure: a nonuniversal (model-dependent) lower-order part and a universal higher-order part that belongs to RMT, and the starting point of the second of these gives an estimation for the Thouless energy. Compared to more standard probes like number variance or the spectral form factor, this approach requires no unfolding procedure.

Moreover, we also improve the understanding about the power-law behavior  $\lambda_k \sim k^{-\alpha}$ . By studying the scree plots of SRPM, unitary spin chain, and non-standard Gaussian  $\beta$  ensembles, we verified the universal exponent  $\alpha$  corresponds only to the parameter  $\beta_2$  in the exponential part of the level spacing distribution in Eq. (8) while being insensitive to the level repulsion parameter  $\beta_1$ , or equivalently, the symmetry of the system. Consequently,  $\alpha$  gives an underestimation for the ergodic-MBL transition point, which suggests a nonergodic behavior that may be attributed to the Griffiths regime.

The existence of a subtle correspondence between the eigenvalues and eigenfunctions is an intriguing property of complex quantum system [66], and there is certainly more hidden information in the eigenvalues deserves to be explored. One immediate direction is to construct an eigenvalue-based time series that is able to read the symmetry of the system (most probably through the level repulsion). It is also possible to apply SVD to non-Hermitian MBL systems with complex eigenvalues [67,68]. It is exciting to see whether such power-law scree plots appear in these systems or not.

## ACKNOWLEDGMENTS

The author acknowledges E. Kanzieper for introducing Refs. [51–53]. This work is supported by the National Natural Science Foundation of China through Grant No.11904069.

- [1] I. V. Gornyi, A. D. Mirlin, and D. G. Polyakov, *Phys. Rev. Lett.* **95**, 206603 (2005); **95**, 046404 (2005).
- [2] D. M. Basko, I. L. Aleiner, and B. L. Altshuler, *Ann. Phys. (NY)* **321**, 1126 (2006).
- [3] J. A. Kjall, J. H. Bardarson, and F. Pollmann, *Phys. Rev. Lett.* **113**, 107204 (2014).
- [4] Z. C. Yang, C. Chamon, A. Hama, and E. R. Mucciolo, *Phys. Rev. Lett.* **115**, 267206 (2015).
- [5] M. Serbyn, A. A. Michailidis, D. A. Abanin, and Z. Papić, *Phys. Rev. Lett.* **117**, 160601 (2016).

- [6] M. Serbyn, Z. Papić, and D. A. Abanin, *Phys. Rev. X* **5**, 041047 (2015).
- [7] H. Kim and D. A. Huse, *Phys. Rev. Lett.* **111**, 127205 (2013).
- [8] J. H. Bardarson, F. Pollmann, and J. E. Moore, *Phys. Rev. Lett.* **109**, 017202 (2012).
- [9] M. Serbyn, Z. Papić, and D. A. Abanin, *Phys. Rev. B* **90**, 174302 (2014).
- [10] C. L. Bertrand and A. M. García-García, *Phys. Rev. B* **94**, 144201 (2016).
- [11] M. Znidaric, T. Prosen, and P. Prelovsek, *Phys. Rev. B* **77**, 064426 (2008).

- [12] V. Oganesyan and D. A. Huse, *Phys. Rev. B* **75**, 155111 (2007).
- [13] Y. Avishai, J. Richert, and R. Berkovits, *Phys. Rev. B* **66**, 052416 (2002).
- [14] N. Regnault and R. Nandkishore, *Phys. Rev. B* **93**, 104203 (2016).
- [15] S. D. Geraedts, R. Nandkishore, and N. Regnault, *Phys. Rev. B* **93**, 174202 (2016).
- [16] V. Oganesyan, A. Pal, and D. A. Huse, *Phys. Rev. B* **80**, 115104 (2009).
- [17] A. Pal and D. A. Huse, *Phys. Rev. B* **82**, 174411 (2010).
- [18] S. Iyer, V. Oganesyan, G. Refael, and D. A. Huse, *Phys. Rev. B* **87**, 134202 (2013).
- [19] D. J. Luitz, N. Laflorencie, and F. Alet, *Phys. Rev. B* **91**, 081103(R) (2015).
- [20] M. Serbyn and J. E. Moore, *Phys. Rev. B* **93**, 041424(R) (2016).
- [21] M. L. Mehta, *Random Matrix Theory* (Springer, New York, 1990).
- [22] F. Haake, *Quantum Signatures of Chaos* (Springer, New York, 2001).
- [23] B. Altshuler, I. Zarekeshev, S. Kotochigova, and B. Shklovskii, *Zh. Eksp. Teor. Fiz.* **94**, 343 (1988) [*Sov. Phys. JETP* **67**, 625 (1988)].
- [24] R. Berkovits, *Phys. Rev. B* **104**, 054207 (2021).
- [25] R. Berkovits, *Phys. Rev. B* **102**, 165140 (2020).
- [26] X. Chen and A. W. W. Ludwig, *Phys. Rev. B* **98**, 064309 (2018).
- [27] A. Chan, A. De Luca, and J. T. Chalker, *Phys. Rev. Lett.* **121**, 060601 (2018).
- [28] P. Sierant, D. Delande, and J. Zakrzewski, *Phys. Rev. Lett.* **124**, 186601 (2020).
- [29] J. Šuntajs, J. Bonča, T. Prosen, and L. Vidmar, *Phys. Rev. E* **102**, 062144 (2020).
- [30] K. Agarwal, S. Gopalakrishnan, M. Knap, M. Müller, and E. Demler, *Phys. Rev. Lett.* **114**, 160401 (2015).
- [31] S. Gopalakrishnan, K. Agarwal, E. A. Demler, D. A. Huse, and M. Knap, *Phys. Rev. B* **93**, 134206 (2016).
- [32] K. Agarwal, E. Altman, E. Demler, S. Gopalakrishnan, D. A. Huse, and M. Knap, *Ann. Phys. (Leipzig)* **529**, 1600326 (2017).
- [33] D. J. Luitz and Y. Bar Lev, *Ann. Phys. (Leipzig)* **529**, 1600350 (2017).
- [34] N. Macé, F. Alet, and N. Laflorencie, *Phys. Rev. Lett.* **123**, 180601 (2019).
- [35] J. M. G. Gomez, R. A. Molina, A. Relano, and J. Retamosa, *Phys. Rev. E* **66**, 036209 (2002).
- [36] V. E. Kravtsov, I. M. Khaymovich, E. Cuevas, and M. Amini, *New J. Phys.* **17**, 122002 (2015).
- [37] R. Fossion, G. Torres Vargas, and J. C. López-Vieyra, *Phys. Rev. E* **88**, 060902(R) (2013).
- [38] G. Torres-Vargas, R. Fossion, C. Tapia-Ignacio, and J. C. López-Vieyra, *Phys. Rev. E* **96**, 012110 (2017).
- [39] G. Torres-Vargas, J. A. Méndez-Bermúdez, J. C. López-Vieyra, and R. Fossion, *Phys. Rev. E* **98**, 022110 (2018).
- [40] A. Relaño, J. M. G. Gómez, R. A. Molina, J. Retamosa, and E. Faleiro, *Phys. Rev. Lett.* **89**, 244102 (2002).
- [41] A. M. García-García, *Phys. Rev. E* **73**, 026213 (2006).
- [42] E. Faleiro, J. M. G. Gómez, R. A. Molina, L. Muñoz, A. Relaño, and J. Retamosa, *Phys. Rev. Lett.* **93**, 244101 (2004).
- [43] A. Relaño, L. Muñoz, J. Retamosa, E. Faleiro, and R. A. Molina, *Phys. Rev. E* **77**, 031103 (2008).
- [44] L. Wang, *Phys. Rev. B* **94**, 195105 (2016).
- [45] C. Wang and H. Zhai, *Phys. Rev. B* **96**, 144432 (2017).
- [46] N. C. Costa, W. Hu, Z. J. Bai, R. T. Scalettar, and R. R. P. Singh, *Phys. Rev. B* **96**, 195138 (2017).
- [47] N. Jiang, S. Ke, H. Ji, H. Wang, Z.-X. Hu, and X. Wan, *Phys. Rev. B* **102**, 115140 (2020).
- [48] F. Alet and N. Laflorencie, *C. R. Phys.* **19**, 498 (2018).
- [49] Á. L. Corps, R. A. Molina, and A. Relaño, *Phys. Rev. B* **102**, 014201 (2020).
- [50] Á. L. Corps, R. A. Molina, and A. Relaño, *SciPost Phys.* **10**, 107 (2021).
- [51] R. Riser, V. Al. Osipov, and E. Kanzieper, *Phys. Rev. Lett.* **118**, 204101 (2017).
- [52] R. Riser, V. Al. Osipov, and E. Kanzieper, *Ann. Phys. (NY)* **413**, 168065 (2020).
- [53] R. Riser and E. Kanzieper, *Ann. Phys. (NY)* **425**, 168393 (2021).
- [54] E. B. Bogomolny, U. Gerland, and C. Schmit, *Eur. Phys. J. B* **19**, 121 (2001).
- [55] H. Hernández-Saldaña, J. Flores, and T. H. Seligman, *Phys. Rev. E* **60**, 449 (1999).
- [56] I. Dumitriu and A. Edelman, *J. Math. Phys. (NY)* **43**, 5830 (2002).
- [57] Y. Y. Atas, E. Bogomolny, O. Giraud, and G. Roux, *Phys. Rev. Lett.* **110**, 084101 (2013).
- [58] P. Sierant and J. Zakrzewski, *Phys. Rev. B* **99**, 104205 (2019).
- [59] V. Khemani, D. N. Sheng, and D. A. Huse, *Phys. Rev. Lett.* **119**, 075702 (2017).
- [60] W.-J. Rao, *J. Phys. A: Math. Theor.* **54**, 105001 (2021).
- [61] E. Bogomolny and M. Sieber, *Phys. Rev. E* **98**, 042116 (2018).
- [62] P. A. Nosov, I. M. Khaymovich, and V. E. Kravtsov, *Phys. Rev. B* **99**, 104203 (2019).
- [63] G. De Tomasi and I. M. Khaymovich, *Phys. Rev. Lett.* **124**, 200602 (2020).
- [64] G. De Tomasi, I. M. Khaymovich, F. Pollmann, and S. Warzel, *Phys. Rev. B* **104**, 024202 (2021).
- [65] B. L. Altshuler, Y. Gefen, A. Kamenev, and L. S. Levitov, *Phys. Rev. Lett.* **78**, 2803 (1997).
- [66] J. T. Chalker, I. V. Lerner, and R. A. Smith, *Phys. Rev. Lett.* **77**, 554 (1996).
- [67] R. Hamazaki, K. Kawabata, and M. Ueda, *Phys. Rev. Lett.* **123**, 090603 (2019).
- [68] L. Sá, P. Ribeiro, and T. Prosen, *Phys. Rev. X* **10**, 021019 (2020).